Iranian Journal of Chemical Engineering
Vol. 15, No. 3 (Summer 2018), IAChE

CFD Simulation of Segregation Behavior of a Ternary Mixture in a Bubbling Fluidized Bed: Effect of Solid Wall Boundary Condition

M. Rasteh [1*], F. Farhadi [2]

[1] Department of Chemical Engineering, Hamedan University of Technology, P.O. Box: 65155-579, Hamedan, Iran
[2] Department of Chemical and Petroleum Engineering, Sharif University of Technology, P.O. Box: 11155, Tehran, Iran

ARTICLE INFO

Article history:
Received: 2018-04-07
Accepted: 2018-07-01

Keywords:
Ternary Mixture,
Segregation,
Boundary Condition,
Bubbling Fuidized Bed,
CFD Simulation

ABSTRACT

The effect of the solid–wall boundary condition on the segregation behavior of a sand ternary mixture differing in size, yet with the same proportion, has been investigated in a gas–solid bubbling fluidized bed. A multi-fluid computational fluid dynamics model incorporating the kinetic theory of granular flow has been used. The mass fraction profiles of different-sized particles along the bed height have been experimentally measured by 'freeze–sieving' method. The simulation results of mass fraction distribution and segregation index have been compared against our experimental data in order to evaluate solid–wall boundary conditions in terms of specularity and particle-wall restitution coefficients. The analysis indicates that the specularity coefficients in the range of 0.5 to 0.9 lead to the satisfactory results, and the best agreement is obtained for φ=0.9, which corresponds to partial–slip wall boundary condition, while the particle–wall restitution coefficient has only negligible effect on the results. In addition, maximum segregation index occurs at specularity coefficient of 0.9 at which the segregation pattern may be affected by simultaneous mechanisms of particles circulation and bubbles rising. The effects of superficial gas velocity on the segregation behavior in bubbling regime have also been studied, and a significant reduction in segregation index has been observed with increasing gas velocity from 1.1 U_{mf} to 1.3 U_{mf}.

1. Introduction

fluidized beds are widely used in the process industry for their performance of effective mixing, high rate of heat and mass transfer, and capability of continuous operation [1]. In most cases, the behaviors of fluidized beds are studied, assuming that particles are monodispersed, characterized by the Sauter mean diameter. However, polydispersed particles with broad size distributions are present in many applications of fluidized beds such as drug manufacturing, polymerization reactors, and coal combustors [2]. Polydispersed systems exhibit different

[*] Corresponding author: mrasteh@hut.ac.ir

hydrodynamic behaviors compared with monodispersed ones because of mixing and segregation effects [3].

In situations where particles of different size ranges are moving relative to each other, a dynamic equilibrium is developed between the competing mixing and segregation mechanisms [4]. This equilibrium leads to a segregation pattern so that large particles can tend to sink at the bottom of the bed, named as 'jetsam', while the small particles tend to float at the top of the bed, called 'flotsam' [5]. The mechanism of segregation mainly depends on superficial gas velocity that can result from a major difference in drag and gravity force between solid particles [6], granular temperature and pressure of particles [7], gas–phase turbulence, particle collisions [8], and bubbles' motion in the bed [9]. Some research results have shown that the lower gas velocity increases segregation, while the higher gas velocity promotes the mixing process [10]. The axial or horizontal segregation pattern can be influenced by key parameters, such as particle size distribution (PSD), particle density distribution, particles shape, particles loading, fluidization regime, gas distributer type, and so on [11].

The popular numerical methods for investigating the different aspects of particle segregation in fluidized beds are based on Eulerian–Lagrangian (discrete element model, DEM) and Eulerian–Eulerian (multi-fluid model, MFM) models via computational fluid dynamics (CFD) simulations [10]. It is well known that the performance of DEM and MFM simulation depends on the proper description of all possible intra– and inter–phase interactions, such as collision and frictional interactions between particles, gas–solid interactions, and interactions between particles and wall [12,13].

The interaction between wall and particles explained as in solid-wall boundary condition is one of the most important parameters that affects the accurate prediction of MFM in fluidized beds [14,15]. The general type of boundary condition commonly used in CFD simulation of fluidization processes was derived by Johnson and Jackson [16] who introduced the specularity coefficient (φ) coefficient to describe the wall boundary conditions. The specularity coefficient determines the shear condition at the walls with the value between 0 for perfectly specular collision (free-slip) and 1 for perfectly diffuse collision (no-slip). The particle–wall restitution coefficient (e_w) is another parameter that affects the solid wall boundary condition. It specifies the dissipation of the solid kinetic energy due to particle-wall collisions. A value of e_w close to unity denotes very low dissipation of kinetic energy.

Although many authors have investigated the impact of solid-wall boundary condition on the hydrodynamics of monodispersed particles in fluidized beds [17,18], few have reported on polydispers systems, which have mainly been limited to binary mixtures. Focusing on the solid wall boundary condition, Zhong et al. [13] studied the mixing/segregation behavior of binary mixtures in bubbling fluidized beds and showed the major impact of specularity coefficient on the segregation of binary particles. The mixing/segregation behavior of binary mixture of biomass and biochar particles in a bubbling fluidized bed was studied by Sharma et al. [19], and the effect of different model parameters, such as solid wall boundary condition, was analyzed via MFM/CFD simulation. They reported that the specularity coefficient had considerable

impact on the segregation rate of particles with different sizes and densities at superficial gas velocities close to minimum fluidization velocity. Geng et al. [20] investigated the effect of solid wall boundary conditions on the MFM results of a pseudo-2D bubbling fluidized bed and reported the importance of the expression under granular temperature and also the specularity coefficient for predicting the mixing behavior.

Although partial-slip [2,4] or no–slip [21,22] wall boundary conditions have been used for the numerical simulation of binary particle mixtures, the effect of wall boundary condition on mixing/segregation of other polydispersed systems, such as ternary particles, is not fully understood. The literature survey shows the lack of available studies on the evaluation of the effects of solid wall boundary condition on mixing/segregation of ternary mixtures in fluidized beds.

The main objective of this paper is to identify and outline the role of solid wall boundary condition as well as superficial gas velocity in mixing/segregation behavior of ternary mixture of sand particles differing in size, yet similar in density in a cylindrical fluidized bed. To this purpose, an Eulerian–Eulerian multi-fluid model incorporating the kinetic theory of granular flow is formulated to simulate the mixing/segregation phenomena. The influence of solid wall boundary condition in terms of specularity coefficient as well as particle–wall restitution coefficient and also the effect of superficial gas velocity on particle segregation behavior, at bubbling regime, is evaluated. The simulation results of axial segregation profile are compared with the experimental data obtained by 'freeze-sieving' method.

2. Experimental setup and procedures

2.1. Apparatus

A schematic diagram of the experimental setup is illustrated in Fig. 1. The experiments were carried out in a cylindrical fluidized bed made of Plexiglas. The characteristics of the main apparatus and technical specification of the experiments are given in Table 1. A plate with standard mesh #170 is considered as the bed material support as well as distributor at the bottom. A compressor (HSS make, model: MICAS-PH-180-1055) with 1000 Lit/min capacity was used to provide air as the fluidizing gas. The regulated air under ambient condition passed through a silica gel tower to dry before being sent through the bed. Two rotameters (accuracy ± 2 % FSD), one for the lower range (0-5 m^3/h) and the other for the higher range (5-20 m^3 /h), monitored the desired airflow rate. The bed pressure drops were recorded using a low-differential pressure transmitter (Kangyu, KYB14A, China). There are two pressure ports located on the bed inlet (just above the distributor) and on the exit section of the bed. The measured pressure drop was converted into voltage signals by a multi-channel pressure signal transmitter and sent to a computer through an A/D converter. Pressure time series were logged at fixed time intervals (50 ms). The particle size distribution (PSD) along the bed height was determined using a sieving shaker machine (AS200 control, Retsch GmbH, Germany) with sieves ranging from 1400 to 63 μm.

2.2. Procedure

A ternary mixture of sand particles composed of three particle sizes (138, 328 and 550 μm) was used as the bed material. The mixture was prepared by mixing the equal proportions of narrow cut particles (33.3 wt %), which

were between two successive standard sieves; 138 μm: between 125-150 μm, 328 μm: between 300-355 μm, and 550 μm: between 500-600 μm. The physical properties of fluidizing gas and ternary mixture are given in Table 2. In order to determine minimum fluidization velocity (U_{mf}), the investigation of characteristic curves (ΔP-U_0) as a classical method for studying hydrodynamics of fluidization process was employed. In this method, the bed was filled by the pre-determined amount of mixture in order to obtain the desired initial bed height (H_0=8 cm). The airflow rate increased step by step, held at each step for 60 s; then, the bed pressure drop was averaged over the last 15 seconds. This process continued until a full fluidization condition, corresponding to a constant pressure drop with further increasing of gas velocity, was attained. The plot of bed pressure drop (ΔP) versus superficial gas velocity (U_0) reveals some hydrodynamic characteristics of fluidized beds such as fluidization regimes and minimum fluidization velocity as described in literature [23].

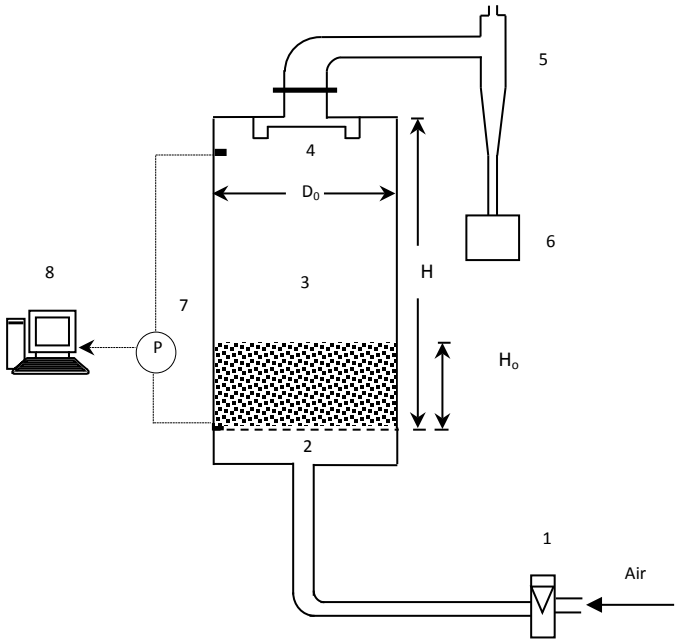

Figure 1. Experimental apparatus: 1) Rotameter, 2) Distributor plate, 3) Bed body, 4) Filter, 5) Cyclone, 6) Receiver, 7) Differential pressure transmitters, and 8) Computer.

Table 1
The apparatus specification and experimental conditions.

Bed diameter (D_0)	18 cm
Bed height (H)	30 cm
Particles height in bed (H_0)	8 cm
Distributor plate	US standard mesh #170
Compressor capacity	1000 Lit/min
Pressure (P)	1 atm
Range of gas velocity (U_0)	0.0605- 0.0715 m/s

Table 2
Physical properties of gas and solid phases.

Phase	Property	Symbol (unit)	Value
gas phase	density	ρ_g (kg/m^3)	1.225
	viscosity	μ_g (pa.s)	1.785×10^{-5}
solid phase	average particle size	$d_{p,avg}$ (μm)	338
	mass composition	x_i	33.3 % of 138 μm, 33.3 % of 328 μm and 33.3 % of 550 μm particles
	particle density	ρ_s (kg/m^3)	2650
	bulk density	ρ_b (kg/m^3)	1680
	particle volume fraction	ε_s	0.635

To carry out axial segregation experiments, the bed was fluidized at a relatively high superficial gas velocity (U_0=2.5 U_{mf}=0.1375 m/s) for time duration of 10 min to ensure perfect mixing and reproducibility of initial condition for desired superficial gas velocities. After the end of mixing time, the air supply was shut off; then, the bed was fluidized at the desired superficial gas velocities (U_0= 0.0605, 0.066 and 0.0715 m/s corresponding to1.1 U_{mf}, 1.2 U_{mf} and 1.3 U_{mf}, respectively) for adequate time (30 min) to ensure reaching steady-state condition. After the segregation time, the air flow rate was abruptly shut off to freeze the bed. The frozen bed was then divided into 8 sections along the bed height (1 cm apart), and the particles were vacuumed out of the each section for sieve analysis and determining powder mass composition along the axial direction, as described in [3,24].

3. CFD model description

A two-dimensional (2D) CFD model based on Eulerian-Eulerian approach (MFM) was developed to simulate the behaviors of the fluidized bed containing the ternary mixture described in the experimental section. In the MFM, the phases act as interpenetrating continua, and the mass and momentum conservation equations in the form of generalized Navier-Stokes equations are solved for each phase. Additional source terms are added to the conservation equations to account for the interactions between the phases. The granular temperature (kinetic energy of particulate phase) and other particulate phase properties are evaluated using the kinetic theory of granular flow (KTGF), which makes an analogy between the particulate phases and the kinetic theory of gases. The set of governing equations of MFM and constitutive equations of gas–solid flow based on KTGF are summarized in Tables 3 and 4, respectively. More details about the governing equations can be found in the literature [14,25].

The 2D CFD simulations were performed by the commercial software package FLUENT 15.0.7 (Ansys Inc.). The phase coupled SIMPLE algorithm was used for pressure-velocity coupling in the transient condition. Second-Order Upwind (SOU) scheme for momentum, turbulence kinetic energy and turbulent dissipation rate, and Least Squares Cell Based for gradient were applied for spatial discretization to obtain more precise results. Fixed option time step with the value of 10^{-4}s was used for transient simulations, and the value of 50 for maximum iteration per time step was set. To attain the steady results for hydrodynamic behaviors and segregation pattern, the simulations were run up to 30s, and the outputs were averaged

over the last 10s. The summarized simulation parameters are given in Table 5.

A no-slip boundary condition for the gas phase and various specularity coefficients (0, 0.2, 0.5, 0.9, 0.95, and 1) and different particle-wall restitution coefficients (0.8, 0.9, and 0.95) for particulate phases were used at the wall to study the effects of solid boundary condition on simulation results. The gas entered only in axial direction at the inlet of the bed, (Dirichlet boundary condition), and superficial gas velocity of U_0= 1.1 U_{mf}, 1.2 U_{mf}, and 1.3 U_{mf} were set as the inlet gas velocity. An outflow boundary condition at the outlet of the bed was used, meaning that the gas velocity gradient was set to zero along the axial direction ($\frac{\partial u_y}{\partial y} = 0$), and atmospheric condition for pressure was also considered. The computational domain was discretized with 13500 cells (2 mm×2 mm). The size of the cells is about 8 times the average particle diameter, which provides enough high resolution for the accurate discretization of the solid phase [18,28].

4. Results and discussion

4.1. Minimum fluidization velocity (U_{mf})

Fig. 2 shows the experimental data and the simulation results of bed pressure drop versus superficial gas velocity for different values of specularity coefficient (φ). The $\Delta P–U_o$ diagram can be subdivided into three main regions corresponding to the different fluidization regimes: (I) fixed bed regime; (II) partially fluidized regime; (III) complete fluidized regime [23]. In the fixed bed region, there is a quasi-linear relationship between gas velocity and bed pressure drop, which shows considerable viscous effects in gas–solid interaction [29]. In the partially fluidized region, the smaller particles begin to fluidize, the viscous effects reduce, and the change in pressure drop with gas velocity is elbow like. In the complete fluidized region, the fluidization of all particles occurs, and the total bed pressure drop, which remains almost constant, is balanced with the particles' weight and the particles-wall friction. The gas velocity corresponding to transition from partially fluidized regime to complete fluidized regime is defined as the minimum fluidization velocity (U_{mf}) [23,29].

Table 3
Governing equations of MFM.

Continuity equations of gas and particulate phase (g for gas and s for particulate)
$\frac{\partial}{\partial t}(\varepsilon_g.\rho_g) + (\nabla.\varepsilon_g.\rho_g.\vec{\mathbf{u}}) = 0$
$\frac{\partial}{\partial t}(\varepsilon_s.\rho_s) + (\nabla.\varepsilon_s.\rho_s.\vec{\mathbf{v}}) = 0$
Momentum equations of gas and particulate phase
$\frac{\partial}{\partial t}(\varepsilon_g.\rho_g.\vec{\mathbf{u}}) + (\nabla.\varepsilon_g.\rho_g.\vec{\mathbf{u}}.\vec{\mathbf{u}}) = -\varepsilon_g\nabla P - \beta(\vec{\mathbf{u}} - \vec{\mathbf{v}}) + \nabla.(\varepsilon_g.\bar{\bar{\tau}}_g) + \varepsilon_g.\rho_g.\vec{\mathbf{g}}$
$\frac{\partial}{\partial t}(\varepsilon_s.\rho_s.\vec{\mathbf{v}}) + (\nabla.\varepsilon_s.\rho_s.\vec{\mathbf{v}}.\vec{\mathbf{v}}) = -\varepsilon_s\nabla P - \nabla P_s - \beta(\vec{\mathbf{u}} - \vec{\mathbf{v}}) + \nabla.(\varepsilon_s.\bar{\bar{\tau}}_s) + \varepsilon_s.\rho_s.\vec{\mathbf{g}}$
$\bar{\bar{\tau}}_g = \mu_g[\nabla.\vec{\mathbf{u}} + (\nabla.\vec{\mathbf{u}})^T] - \frac{2}{3}\nabla.\vec{\mathbf{u}}\,\bar{\bar{I}}$
$\bar{\bar{\tau}}_s = \mu_s[\nabla.\vec{\mathbf{v}} + (\nabla.\vec{\mathbf{v}})^T] + \left(\lambda_s - \frac{2}{3}\mu_s\right)\nabla.\vec{\mathbf{v}}\,\bar{\bar{I}}$
Granular temperature equation
$\frac{3}{2}\left[\frac{\partial}{\partial t}(\varepsilon_s\,\rho_s\Theta) + \nabla.(\varepsilon_s\,\rho_s\Theta\,\vec{\mathbf{v}})\right] = (-P_s\,\bar{\bar{I}} + \bar{\bar{\tau}}_s):\nabla\vec{\mathbf{v}} + \nabla.(k_{\Theta s}\nabla.\Theta) - \gamma_{\Theta s} + \emptyset_{\mathbf{gs}}$

Table 4
Constitutive equations of gas-solid flow.

Solids pressure [26]
$P_s = \rho_s \varepsilon_s \Theta + 2 g_0 \rho_s {\varepsilon^2}_s \Theta (1 + e_s)$
Solids bulk viscosity [4]
$\lambda_s = \frac{4}{3} \varepsilon_s \rho_s d_p g_0 (1 + e_s) \sqrt{\frac{\Theta}{\pi}}$
Solids shear viscosity
$\mu_s = \mu_{s,col} + \mu_{s,kin} + \mu_{s,fr}$
Collisional viscosity [1]
$\mu_{s,col} = \frac{4}{5} {\varepsilon_s}^2 \rho_s d_p g_0 (1 + e_s) \sqrt{\frac{\Theta}{\pi}}$
Kinetic viscosity [1]
$\mu_{s,kin} = \frac{10}{96} \sqrt{\Theta \pi} \frac{\rho_s d_p}{(1 + e_s) g_0} \left[1 + \frac{4}{5} g_0 \varepsilon_s (1 + e_s)\right]^2$
Frictional viscosity [27]
$\mu_{s,fr} = \frac{P_s \sin\phi}{\sqrt{4 I_{2D}}}$
Diffusion coefficient of granular energy [1]
$k_{\Theta s} = 2 {\varepsilon_s}^2 \rho_s d_p g_0 (1 + e_s) \sqrt{\frac{\Theta}{\pi}} + \frac{150 \sqrt{\Theta \pi} \rho_s d_p}{384 (1 + e_s) g_0} \left[1 + \frac{6}{5} g_0 \varepsilon_s (1 + e_s)\right]^2$
Collisional energy dissipation [26]
$\gamma_{\Theta s} = 12 (1 - {e_s}^2) \frac{{\varepsilon_s}^2 \rho_s g_0}{d_p \sqrt{\pi}} \Theta^{\frac{3}{2}}$
Radial distribution function [26]
$g_0 = \left[1 - (\frac{\varepsilon_s}{\varepsilon_{s,max}})^{\frac{1}{3}}\right]^{-1}$
Transfer of kinetic energy between phases [1]
$\emptyset_{gs} = -3 \beta \Theta$
k–ε Turbulence model
Gas viscosity $\mu_g = \mu_{l,g} + \mu_{t,g}$, $\mu_{t,g} = C_\mu \varepsilon_g \rho_g \frac{K}{\epsilon}$ Turbulence Kinetic energy $\frac{\partial}{\partial t}(\rho_g K) + \nabla.(\rho_g \vec{\mathbf{u}} K) = \nabla.\left(\frac{\mu_{t,g}}{\sigma_k} K\right) + G_{k,g} - \rho_g \epsilon + \rho_g \Pi_{k,g}$ Turbulence dissipation rate $\frac{\partial}{\partial t}(\rho_g \epsilon) + \nabla.(\rho_g \vec{\mathbf{u}} \epsilon) = \nabla.\left(\frac{\mu_{t,g}}{\sigma_\epsilon} \epsilon\right) + \frac{\epsilon}{K}(C_{1\epsilon} G_{k,g} - C_{2\epsilon} \rho_g \epsilon) + \rho_g \Pi_{\epsilon,g}$ where $G_{k,g} = \mu_{t,g}\left(\nabla \vec{\mathbf{u}} + (\nabla \vec{\mathbf{u}})^T\right) : \nabla \vec{\mathbf{u}}$ $C_\mu = 0.09,\ C_{1\epsilon} = 1.44,\ C_{2\epsilon} = 1.92,\ \sigma_k = 1,\ \sigma_\epsilon = 1.3$

Table 5
The simulation parameters.

Hydrodynamic model		Eulerian–Eulerian, multi-fluid model
Primary phase	phase1: air	ρ_g= 1.225 kg/m^3, μ_g=1.785×10^{-5} pa.s
Secondary phases	phase 2: sand	d_p =138 μm, ρ_s=2650 kg/m^3, ε_1= 0.217
	phase 3: sand	d_p =328 μm, ρ_s=2650 kg/m^3, ε_2= 0.217
	phase 4: sand	d_p =550 μm, ρ_s=2650 kg/m^3, ε_3= 0.217
viscosity model		Standard κ–ε
drag models		Gidaspow
particle–particle restitution coefficient		0.8, 0.9 and 0.95
granular viscosity		Gidaspow
granular bulk viscosity		Lun et al.
frictional viscosity		Schaeffer
angel of internal friction		30^o
friction Packing limit		0.61
solid pressure		Lun et al.
radial distribution		Lun et al.
maximum packaging limit		0.67
specularity coefficient		0, 0.2, 0.5, 0.9, 0.95 and 1
superficial gas velocities		U_0= 0.0605, 0.066 and 0.0715 m/s
initial bed height		8 cm

As seen in Fig. 2, although the variation of pressure drops with gas velocity is similar for all values of specularity coefficient, the total bed pressure drop (ΔP_{max}) and U_{mf} increase with increasing specularity coefficient, albeit the change in U_{mf} with φ in the range of 0 to 1 is relatively small (from 0.05 to 0.059 m/s). The increase of ΔP_{max} and U_{mf} with φ is due to the increase of particles-wall friction. A lower friction results in a lower wall shear stress, which consequently leads to the lower flow resistance for the particles to move closer to the wall and the smoother fluidization [14]. Of note, since measuring φ is not possible in experiments, its value is specified by fitting the simulation results to the experimental data [13]. The comparison of experimental and simulation results of U_{mf} and ΔP_{max} for φ=0, 0.2, 0.5, 0.9, 0.95, and 1 is given in Table 6. According to Table 6, the specularity coefficients in the range of 0.5 to 0.9 lead to the satisfactory results, and the best agreement (relative error 1.8 % for U_{mf} and -0.6 % for ΔP_{max}) is obtained for φ=0.9, which corresponds to partial–slip wall boundary condition for the solid particles.

Table 6
The comparison of experimental data and simulation results of U_{mf} and ΔP_{max} for different specularity coefficients.

Experimental			Simulation			
	U_{mf} (m/s)	ΔP_{max} (Pascal)	U_{mf} (m/s)		ΔP_{max} (Pascal)	
			value	% deviation	value	% deviation
φ=0	0.055	1680	0.05	-9.1	1505	-10.4
φ=0.2			0.053	-3.6	1583	-5.77
φ=0.5			0.054	-1.8	1622	-3.45
φ=0.9			0.056	1.8	1670	-0.60
φ=0.95			0.057	3.6	1715	2.08
φ=1			0.059	7.3	1770	5.36

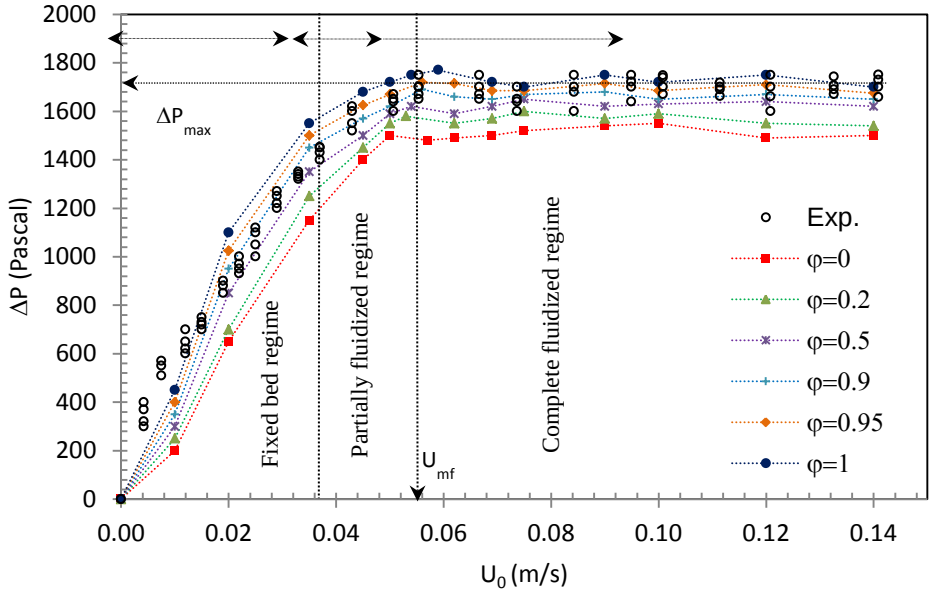

Figure 2. Experimental and simulation results of bed pressure drop versus superficial gas velocity for different values of specularity coefficients.

4.2. Effects of specularity coefficient on segregation pattern

The simulation results versus experimental data for axial composition profiles of small-, medium-, and large-sized particles for different values of specularity coefficient at U_0=1.1 U_{mf} (0.0605 m/s) are illustrated in Fig. 3. In these plots, for a specified particle size, the more vertical line indicates less variation of axial composition, thus representing a slight particles segregation (good mixing), whereas the step–like line indicates an intense particles segregation. As seen in Fig.3, the increase of specularity coefficient in the range of 0 to 0.9 leads to an apparent increase in the composition variations of particles along the bed height; however, the reverse trend is observed for specularity coefficient in the range of 0.9 to 1. These results can be explained as follows: for specularity coefficient between 0 and 0.9, the mechanism of segregation is affected by gulf–effect (particles circulation) with upward flow of particles in the central region and downward flow near the walls. The increasing specularity coefficient reduces particles circulation [30], leading to more intense segregation. For specularity coefficient between 0.9 and 1, the rising bubbles control the segregation mechanism [31]. Although the relatively high particle–wall shear stress leads to the formation of a stagnant layer of particles near the wall that, in turn, reduces particles circulation and increases particles' segregation, formation and rising of the bigger bubbles with higher frequencies promotes particles mixing [32]. It can also be seen from Fig. 3 that the behavior of medium-sized particles is almost similar to that of large particles for all values of specularity coefficients. By comparing the deviations of simulation results of axial composition profiles for different specularity coefficients from experimental data in Table 7, it is clear that the specularity coefficient of 0.9 with average deviation of 6.2 % provides the best agreement with experimental data.

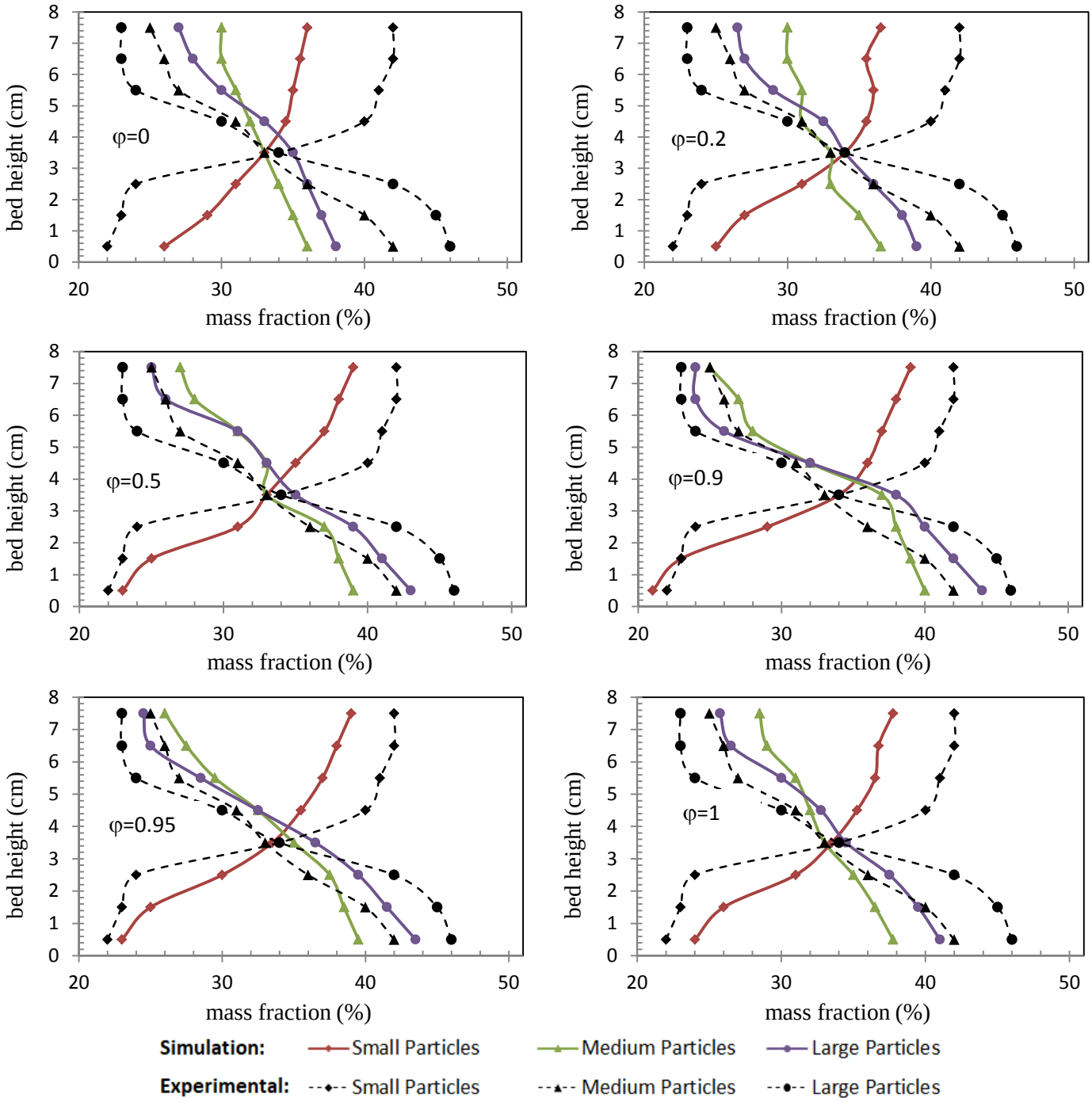

Figure 3. Axial composition profiles of different particle sizes for different values of specularity coefficients.

Table 7
Average absolute deviations of axial mass fraction for particles of different sizes.

Particle size	Specularity coefficient					
	φ=0	φ=0.2	φ= 0.5	φ=0.9	φ=0.95	φ=1
small	16.8	14.0	10.5	7.7	9.7	12.3
medium	10.7	10.5	6.5	4.5	5.5	8.2
large	15.8	13.4	10.8	6.4	8.6	12.1
Average deviation (%)	**14.4**	**12.6**	**9.3**	**6.2**	**7.9**	**10.9**

Besides the analysis of axial composition profiles for different particle sizes, the extent of particles segregation can be described using a single integrated parameter, called segregation index (*s*). The axial compositions of both small- and large-sized particles are employed to define the segregation index, described as [3,33]:

$$s = \frac{S - 1}{S_{max} - 1} \quad (1)$$

Parameter S in numerator of Eq. 1 is the ratio of average heights of the small- and large-sized particles, and it is representative of actual amount of segregation:

$$S = \frac{h_{small}}{h_{large}} \quad (2)$$

where h_{small} and h_{large} are the average dimensionless heights of the small- and large-sized particles, specified as follows:

$$h_{small} = \sum_i x_{small,i} * h_i \quad (3)$$

$$h_{large} = \sum_i x_{large,i} * h_i \quad (4)$$

where h_i denotes the dimensionless height of each axial section that is vacuumed out to determine the composition of each class of particle sizes (x_i).

Parameter S_{max} in denominator of Eq. 1 indicates the maximum amount of segregation that corresponds to the state in which small particles are completely accumulated in the top portion, while the large particles are all collected in the bottom portion of the bed as shown in Fig. 4.

$$S_{max} = \frac{h_{small,max}}{h_{large,min}} \quad (5)$$

$$h_{small,max} = x_{large} + x_{medium} + 0.5 * x_{small} = 1 - x_{small} + 0.5 * x_{small} = 1 - 0.5 * x_{small} \quad (6)$$

$$h_{large} = 0.5 * x_{large} \quad (7)$$

$$S_{max} = \frac{1 - 0.5 * x_{small}}{0.5 * x_{large}} = \frac{2 - x_{small}}{x_{large}} \quad (8)$$

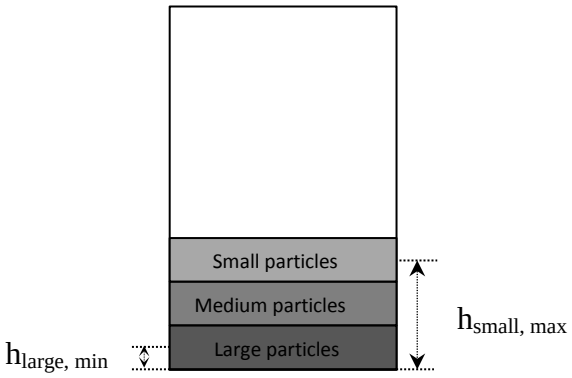

Figure 4. The condition of maximum segregation.

Based on the definition of segregation index (*s*) in Eq.1, *s*=1 refers to perfect particles segregation, whereas *s*=0 denotes perfect particles mixing or no segregation.

Fig. 5 shows experimental value versus simulation results of segregation index obtained by Eq.1 for different values of specularity coefficient at U_0=1.1 U_{mf} (0.0605 m/s). It is clear that the maximum segregation index occurs at specularity coefficient of 0.9 at which the segregation pattern may be affected by simultaneous mechanisms of particles circulation and rising bubbles. It is also seen that the simulations below predict

the segregation indexes for all specularity coefficients that can be attributed to the effects of particles shape, particle–particle frictions, and inter–particle forces, which cannot be included in the CFD simulation.

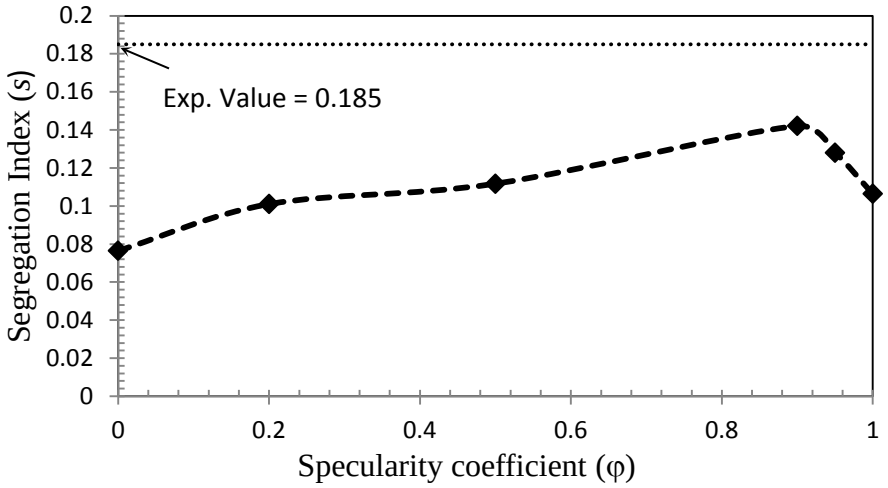

Figure 5. Segregation index for different values of specularity coefficient.

4.3. Effects of particle–wall restitution coefficient on segregation pattern

In order to study the effect of particle-wall restitution coefficient (e_w) which quantifies the dissipation of particles kinetic energy due to collisions with the wall, the simulations were executed using three values of e_w (0.8, 0.9, and 0.95). Fig. 6 shows the simulation and experimental results of axial composition profiles for small-, medium-, and large-sized particles for different particle-wall restitution coefficients at U_0=1.1 U_{mf}. Although reducing e_w will increase the dissipation of particles kinetic energy, leading to a decrease in granular temperature and an increase in solid volume fraction at the wall [28], for e_w values used in this study, the effect of e_w on the axial composition profiles for different particle sizes is negligible. As seen in Fig. 6, no evident differences are observed for the predicted results of e_w= 0.8, 0.9 and 0.95 so that the profiles can be nearly overlapped and are in good agreement with the experimental data. This result is consistent with the findings of Li et al. [28] and Zhong et al. [13], indicating that the particle-wall restitution plays only a minor role in numerical simulation of bubbling fluidized beds.

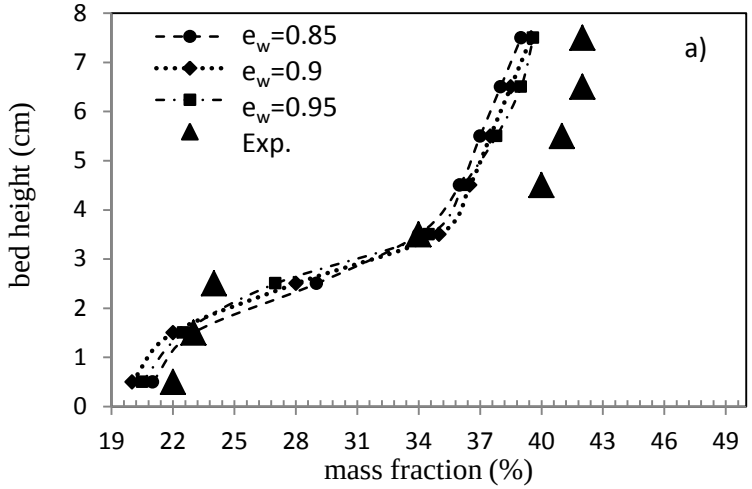

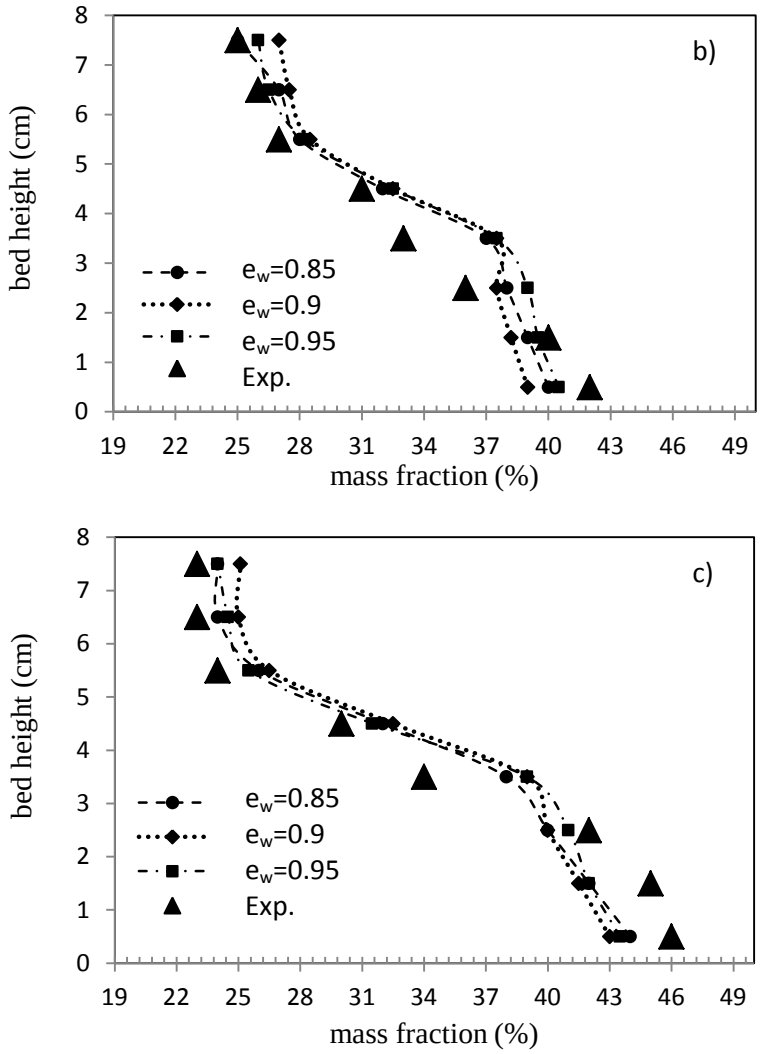

Figure 6. Axial composition profiles of different particle sizes for different values of particle–wall restitution coefficients, a) small, b) medium and c) large particles.

4.4. Effect of superficial gas velocity on segregation pattern

Fig. 7 shows the contours of volume fraction for the gas and solid phases at different superficial gas velocities: U_0= 1.1 U_{mf} (0.0605 m/s), 1.2 U_{mf} (0.066 m/s), and 1.3 U_{mf} (0.0715 m/s) when specularity coefficient and particle-wall restitution coefficient are both set to 0.9. This range of gas velocity is selected to ensure staying in bubbling regime. In fully bubbling fluidized beds, the mixing and segregation pattern is intensely affected by the dynamic behaviors of bubbles [20]. The particles in the wake region of bubbles travel towards the top of bed, resulting in axial mixing, while as bubbles rise, the particles fall down around the bubbles, leading to axial segregation. The mixing and segregation pattern of particles in the bubbling fluidized bed is determined by the dynamic equilibrium of these two phenomena. As seen in Fig. 7, particle mixing is promoted by increasing the gas velocity that results in formation of bigger bubbles with higher frequencies. At superficial gas velocity of U_0= 1.1 U_{mf} (Fig. 7-a), a quasi-stagnant layer of large- and medium-sized particles with no bubble is formed in the lower region of the bed, while small bubbles are observed in the higher zone which is

mainly composed of small particles. In the absence of bubbles in the quasi-stagnant layer, there is no mechanism present to carry the particles to the upper zone of the bed, which indicates the significant role of bubbles for particles mixing in fluidized beds. For this gas velocity, a strong segregation of small particles takes place in the bed, and significant non-homogeneity of the axial particle composition is observed. Increasing the superficial gas velocity to U_0= 1.2 U_{mf} (Fig. 7-b) expands the quasi-stagnant layer that leads to the formation of bubbles in the lower region of the bed. The bubbles act as a vehicle to transport the medium- and large-sized particles to the higher region of the bed. The bubbles get bigger as they ascend and improve the mixing process. The further increase of the gas velocity to U_0= 1.3 U_{mf} (Fig. 7-c) results in the bigger bubbles with higher frequencies that form at the bottom of bed. These bubbles enhance the mixing process so that the particles with different sizes are almost distributed everywhere in the bed.

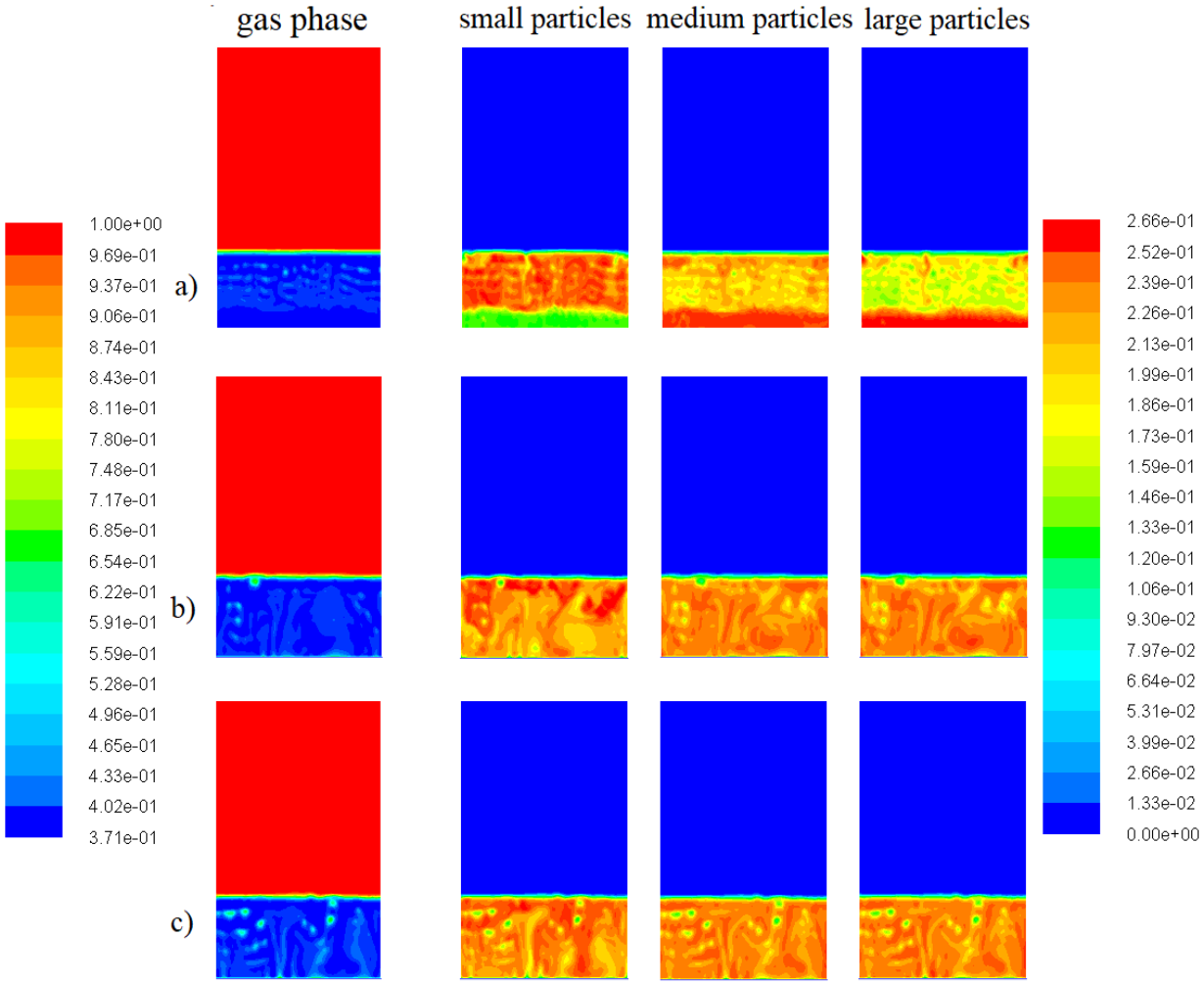

Figure 7. The contour plots of volume fractions for different phases at different superficial gas velocities at t= 25s: a) U_0= 1.1 U_{mf} (0.0605m/s), b) 1.2 U_{mf} (0.066m/s), and c) 1.3 U_{mf} (0.0715m/s).

The time–dependent simulation results versus steady-state experimental values for the segregation index at different superficial gas velocities are presented in Fig. 8. It is seen that the simulation results are close to steady state after approximately 20s from the

beginning of the simulations. A significant reduction in segregation index is observed with increasing gas velocity from 1.1 U_{mf} to 1.3 U_{mf}. As mentioned earlier, in this range of gas velocity, the bubbling regime is observed, and the increase of gas velocity leads to producing the bubbles with larger sizes which rise faster through the bed, causing bed mixing throughout. The comparison of the time-averaged simulation results (between 20 to 30 second) and experimental values of segregation index is given in Table 8. As it can be seen, the deviation of the simulation results from experimental values is reduced at higher superficial gas velocity. This is the reason why, at higher gas velocities, the particles away from each other and the bed expand, leading to a decrease in the particle–particle friction. Since the particle–particle friction, with a large influence on the particles' mixing behavior, is not incorporated in MFM/CFD simulation [34], better agreement between simulation results and experimental data is obtained at a higher gas velocity.

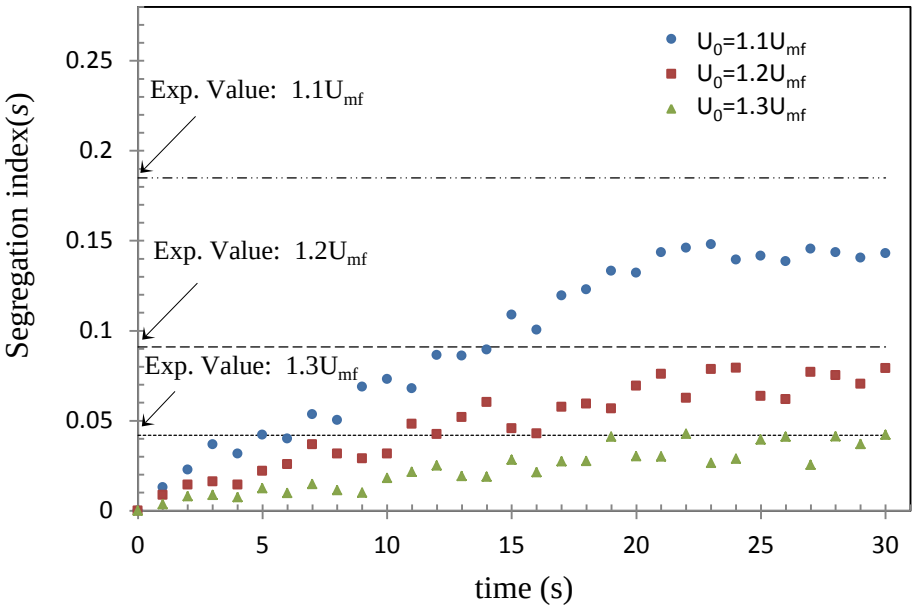

Figure 8. Time-dependent segregation index for different superficial gas velocities.

Table 8
A comparison of simulation results and experimental value for segregation index.

Superficial gas velocity	Experimental value	Simulation result	Absolute deviation
1.1 U_{mf}	0.185	0.142	30.2 %
1.2 U_{mf}	0.091	0.072	26.1 %
1.3 U_{mf}	0.042	0.035	20 %

5. Conclusions

In an attempt to elucidate the significance of the solid-wall boundary condition in prediction of segregation behavior of a ternary mixture in a gas-solid bubbling fluidized bed, CFD simulations were conducted using a multi-fluid model incorporating the kinetic theory of granular

flow. Several simulations with different values of specularity coefficient (φ=0, 0.2, 0.5, 0.9, 0.95 and 1) and different values of particle-wall restitution (e_w=0.8, 0.9 and 0.95) were performed. The simulation results of the bed pressure drop, mass fraction distributions of the different-sized particles along the bed height, and segregation index were compared with experimental data. It was shown that the specularity coefficient had a significant influence on the segregation pattern, and the best agreement between simulation and experimental data obtained by the 'freeze-sieving' method was found at specularity coefficient of 0.9. However, the particle-wall restitution coefficient had only a negligible effect on the results.

The investigation of effects of superficial gas velocity on the segregation behavior in bubbling regime showed an obvious reduction in the segregation index with increasing superficial gas velocity. Increasing the superficial gas velocity from 1.1 U_{mf} (0.0605 m/s) to 1.3 U_{mf} (0.0715 m/s) leads to the expansion of the quasi-stagnant layer of medium- and large-sized particles and to the formation of bubbles in the lower region of the bed. The bubbles get larger when they rise and act as a carrier to transport the medium and large particles to the upper region of the bed. It was indicated that the mechanism of particles segregation was affected by the bubbles dynamics so that the larger gas velocity implied the larger and faster moving bubbles that reduced the segregation index.

Nomenclature

d_p	particle diameter [m].
e_s	restitution coefficient of particle-particle.
e_w	wall-particle restitution coefficient.
$\vec{g}$	gravity [$m.s^{-2}$].
g_0	radial distribution function.
I_{2D}	second invariant of the deviatoric stress tensor.
C_μ, $C_{1\epsilon}$, $C_{2\epsilon}$, σ_k, σ_ϵ	turbulence model coefficients.
$G_{k,g}$	turbulence kinetic energy production [$kg.m^{-1}.s^{-3}$].
$\bar{\bar{I}}$	unit tensor.
P_s	solid pressure [$kg.m^{-1}.s^{-2}$].
$\vec{u}$	gas velocity vector [$m.s^{-1}$].
$\vec{v}$	particle velocity vector [$m.s^{-1}$].
D_0	bed diameter.
H	bed height.
H_0	particles height in bed.
s	segregation index.
U_{mf}	minimum fluidization velocity.
K	turbulent kinetic energy of gas phase [$m^2.s^{-2}$].
P	pressure [$kg.m^{-1}.s^{-2}$].

Greek letters

Θ	granular temperature [$m^2.s^{-2}$].
$\Pi_{K,g}$, $\Pi_{\epsilon,g}$	influence of the dispersed phases on the continuous phase.
$\mu_{l,g}$	gas molecular viscosity [$kg.m^{-1}.s^{-1}$].
$\mu_{s,col}$	collisional viscosity of solid [$kg.m^{-1}.s^{-1}$].
$\mu_{s,fr}$	frictional viscosity of solid [$kg.m^{-1}.s^{-1}$].
$\mu_{s,kin}$	kinetic viscosity of solid [$kg.m^{-1}.s^{-1}$].
λ_s	bulk viscosity of solid [$kg.m^{-1}.s^{-1}$].
μ_s	shear viscosity of solid [$kg.m^{-1}.s^{-1}$].
$\mu_{t,g}$	gas turbulent viscosity [$kg.m^{-1}.s^{-1}$].
μ_g	gas viscosity [$kg.m^{-1}.s^{-1}$].
Θ_w	granular temperature at wall [$m^2.s^{-2}$].
$\bar{\bar{\tau}}_g$, $\bar{\bar{\tau}}_s$	stress tensor for gas and solid phase, respectively [$kg.m^{-1}.s^{-2}$].
$\emptyset_{gs}$	transfer of kinetic energy between

	phases [$\mathrm{kg.m^{-1}.s^{-3}}$].
$k_{\Theta s}$	diffusion coefficient of granular energy [$\mathrm{kg.m^{-1}.s^{-1}}$].
$\gamma_{\Theta s}$	collisional energy dissipation [$\mathrm{kg.m^{-1}.s^{-3}}$].
$\varepsilon_g, \varepsilon_s$	volume fraction of gas and solid respectively.
$\varepsilon_{s,max}$	maximum packing limit of solids.
ρ_g , ρ_s	gas and solid density [$\mathrm{kg.m^{-3}}$].
β	momentum interphase exchange coefficient [$\mathrm{kg.m^{-3}.s^{-1}}$].
φ	specularity coefficient.
ϵ	turbulence dissipation energy of gas phase [$\mathrm{m^2.s^{-3}}$].

References

[1] Gidaspow, D., Multiphase flow and fluidization: Continuu and kinetic theory descriptions, Academic Press, (1994).

[2] Huilin, L., Yunhua, Z., Ding, J., Gidaspow, D. and Wei, L., "Investigation of mixing/segregation of mixture particles in gas-solid fluidized beds", *Chem. Eng. Sci.*, **62**, 301 (2007).

[3] Chew, J. W., Wolz, J. R. and Hrenya, C. M., "Axial segregation in bubbling gas-fluidized beds with Gaussian and lognormal distributions of Geldart Group B particles", *AIChE J.*, **56**, 3049 (2010).

[4] Huilin, L., Yurong, H., Gidaspow, D., Lidan, Y. and Yukun, Q., "Size segregation of binary mixture of solids in bubbling fluidized beds", *Powder Technol.*, **134**, 86 (2003).

[5] Nienow, A. W., Rowe, P. N. and Cheung, L. Y. -L., "A quantitative analysis of the mixing of two segregating powders of different density in a gas-fluidised bed", *Powder Technol.*, **20**, 89 (1978).

[6] Cluet, B., Mauviel, G., Rogaume, Y., Authier, O. and Delebarre, A., "Segregation of wood particles in a bubbling fluidized bed", *Fuel Process. Technol.*, **133**, 80 (2015).

[7] van Wachem, B. G. M., Schouten, J. C., van den Bleek, C. M., Krishna, R. and Sinclair, J. L., "Comparative analysis of CFD models of dense gas-solid systems", *AIChE J.*, **47**, 1035 (2001).

[8] Joseph, G. G., Leboreiro, J., Hrenya, C. M. and Stevens, A. R., "Experimental segregation profiles in bubbling gas-fluidized beds", *AIChE J.*, **53**, 2804 (2007).

[9] Rowe, P. N. and Nienow, A. W., "Particle mixing and segregation in gas fluidised beds: A review", *Powder Technol.*, **15**, 141 (1976).

[10] Zhang, Y., Zhao, Y., Lu, L., Ge, W., Wang, J. and Duan, C., "Assessment of polydisperse drag models for the size segregation in a bubbling fluidized bed using discrete particle method", *Chem. Eng. Sci.*, **160**, 106 (2017).

[11] Jang, H. T., Park, T. S. and Cha, W. S., "Mixing-segregation phenomena of binary system in a fluidized bed", *J. Ind. Eng. Chem.*, **16**, 390 (2010).

[12] Herzog, N., Schreiber, M., Egbers, C. and Krautz, H. J., "A comparative study of different CFD-codes for numerical simulation of gas-solid fluidized bed hydrodynamics", *Comput. Chem. Eng.*, **39**, 41 (2012).

[13] Zhong, H., Gao, J., Xu, C. and Lan, X., "CFD modeling the hydrodynamics of binary particle mixtures in bubbling fluidized beds: Effect of wall boundary condition", *Powder Technol.*, **230**, 232 (2012).

[14] Lan, X., Xu, C., Gao, J. and Al-Dahhan, M., "Influence of solid-phase wall boundary condition on CFD simulation

of spouted beds", *Chem. Eng. Sci.*, **69** 419 (2012).

[15] Zhou, X., Gao, J., Xu, C. and Lan, X., "Effect of wall boundary condition on CFD simulation of CFB risers", *Particuology*, **11**, 556 (2013).

[16] Johnson, P. C. and Jackson, R., "Frictional-collisional constitutive relations for granular materials, with application to plane shearing", *J. Fluid Mech.*, **176**, 67 (1987).

[17] Loha, C., Chattopadhyay, H. and Chatterjee, P. K., "Euler-euler CFD modeling of fluidized bed: Influence of specularity coefficient on hydrodynamic behavior", *Particuology*, **11**, 673 (2013).

[18] Bahramian, A., Olazar, M. and Ahmadi, G., "Effect of slip boundary conditions on the simulation of microparticle velocity fields in a conical fluidized bed", *AIChE J.*, **59**, 4502 (2013).

[19] Sharma, A., Wang, S., Pareek, V., Yang, H. and Zhang, D., "CFD modeling of mixing/segregation behavior of biomass and biochar particles in a bubbling fluidized bed", *Chem. Eng. Sci.*, **106**, 264 (2014).

[20] Geng, S., Jia, Z., Zhan, J., Liu, X. and Xu, G., "CFD modeling the hydrodynamics of binary particle mixture in pseudo-2D bubbling fluidized bed: Effect of model parameters", *Powder Technol.*, **302**, 384 (2016).

[21] Gao, J., Lan, X., Fan, Y., Chang, J., Wang, G., Lu, C. and Xu, C., "Hydrodynamics of gas-solid fluidized bed of disparately sized binary particles", *Chem. Eng. Sci.*, **64**, 4302 (2009).

[22] Coroneo, M., Mazzei, L., Lettieri, P., Paglianti, A. and Montante, G., "CFD prediction of segregating fluidized bidisperse mixtures of particles differing in size and density in gas-solid fluidized beds", *Chem. Eng. Sci.*, **66**, 2317 (2011).

[23] Rasteh, M., Farhadi, F. and Bahramian, A., "Hydrodynamic characteristics of gas-solid tapered fluidized beds: Experimental studies and empirical models", *Powder Technol.*, **283**, 355 (2015).

[24] Schaafsma, S. H., Marx, T. and Hoffmann, A. C., "Investigation of the particle flowpattern and segregation in tapered fluidized bed granulators", *Chem. Eng. Sci.*, **61**, 4467 (2006).

[25] Almuttahar, A. and Taghipour, F., "Computational fluid dynamics of high density circulating fluidized bed riser: Study of modeling parameters", *Powder Technol.*, **185**, 11 (2008).

[26] Lun, C. K. K., Savage, S. B., Jeffrey, D. J. and Chepurniy, N., "Kinetic theories for granular flow: Inelastic particles in Couette flow and slightly inelastic particles in a general flowfield", *J. Fluid Mech.*, **140**, 223 (1984).

[27] Schaeffer, D. G., "Instability in the evolution equations describing incompressible granular flow", *J. Differ. Equ.*, **66**, 19 (1987).

[28] Li, T., Grace, J. and Bi, X., "Study of wall boundary condition in numerical simulations of bubbling fluidized beds", *Powder Technol.*, **203**, 447 (2010).

[29] Khani, M. H., "Models for prediction of hydrodynamic characteristics of gas-solid tapered and mini-tapered fluidized beds", *Powder Technol.*, **205**, 224 (2011).

[30] Benyahia, S., Syamlal, M. and O'Brien, T. J., "Study of the ability of multiphase continuum models to predict core-annulus flow", *AIChE J.*, **53**, 2549 (2007).

[31] Zhang, Y., Zhao, Y., Lu, L., Ge, W., Wang, J. and Duan, C., "Assessment of polydisperse drag models for the size segregation in a bubbling fluidized bed using discrete particle method", *Chem. Eng. Sci.*, **160**, 106 (2017).

[32] Sun, J. and Battaglia, F., "Hydrodynamic modeling of particle rotation for segregation in bubbling gas-fluidized beds", *Chem. Eng. Sci.*, **61**, 1470 (2006).

[33] Olaofe, O. O., Patil, A. V., Deen, N. G., van der Hoef, M. A. and Kuipers, J. A. M., "Simulation of particle mixing and segregation in bidisperse gas fluidized beds", *Chem. Eng. Sci.*, **108**, 258 (2014).

[34] van der Hoef, M. A., van Sint Annaland, M., Deen, N. G. and Kuipers, J. A. M., "Numerical simulation of Dense gas-solid fluidized beds: A multiscale modeling strategy", *Annu. Rev. Fluid Mech.*, **40**, 47 (2008).